

Steady flows inside and around a fluid sphere at low Reynolds numbers

By D. L. R. OLIVER AND J. N. CHUNG

Department of Mechanical Engineering, Washington State University,
Pullman, Washington 99164-2920

(Received 30 November 1983 and in revised form 14 November 1984)

The effects of internal circulation in bubbles and droplets have been analysed by means of a semi-analytical series-truncation method. The equations of motion are transformed into a series of coupled, ordinary, nonlinear differential equations by use of orthogonal sets. These infinite-series equations are then truncated adequately and solved numerically. Using this series-truncation method, we have evaluated the effects of different ratios (between the continuous and dispersed phases) of both density and viscosity for the flows of low Reynolds numbers. For all the density ratios investigated, the density difference has almost no effect on the drag coefficient at low Reynolds numbers. The shear stress and the drag coefficient increase with increasing viscosity ratio of droplet to ambience and decrease with increasing Reynolds number.

1. Introduction

This investigation is aimed at the theoretical evaluation of the flow patterns, both inside and outside of a fluid sphere moving in an immiscible fluid at low Reynolds numbers. The analyses were made through an efficient semi-analytical numerical procedure. Solutions to the problem provide the flow patterns inside and outside of the sphere, the drag coefficient, and the effects of viscosity ratio and density ratio on the motion of a fluid sphere.

The current problem is the study of the steady incompressible axially symmetric viscous flow over a fluid sphere which is simultaneously experiencing an internal motion induced by the external flow. In the past, extensive work has been done in the area of flow over solid spheres and gas bubbles, where the internal motion is either absent or unimportant. In the low-Reynolds-number flow, Proudman & Pearson (1957) successfully refined Stokes' creeping-flow solution through the matched asymptotic expansions, and their work has been further improved by Chester & Breach (1963). Typical numerical solutions for flow over solid spheres were given by Dennis & Walker (1964), Hamielec, Hoffman & Ross (1967), and LeClair, Hamielec & Pruppacher (1970), for a wide range of Reynolds numbers. Maxworthy (1965), Pruppacher & Steinberger (1968), Beard & Pruppacher (1969), and Pruppacher, LeClair & Hamielec (1970) have published experimental results and showed comparisons with theoretical results.

For fluid drops or gas bubbles moving in another fluid of comparable or higher viscosity, results have been developed for high Reynolds numbers, where the major simplification is the existence of thin viscous boundary layers on both sides of the interfaces, with the flow being slightly perturbed from inviscid solutions. Typical papers in this area are by Moore (1963), Chao (1962), Winnikow & Chao (1966), and Harper & Moore (1968). Both Chao (1962) and Winnikow & Chao (1966) contain

technical errors as pointed out by Harper (1972). The experimental work of Winnikow & Chao (1966) is considered very good. However, the theory of all the above is not applicable to liquid spheres in a low-viscosity environment, and this is due to the difference in viscosity ratio and density ratio. Prakash & Sirignano (1980) have published an approximate method for liquid fuel spheres in a gas atmosphere, and the flow pattern is close to that found for flow over solid spheres. The internal flow of a liquid droplet was found to be two orders of magnitude slower than that of a gas bubble. A lot of work with liquid droplets has been done by meteorologists. For example, see McDonald (1954), Pruppacher & Beard (1970) and Pruppacher & Klett (1978). A closed-form solution for flow over a fluid sphere in the creeping-flow range was provided by Rybczynski (1911) and Hadamard (1911). Harper (1972) provides us with an excellent review for motions of bubbles and droplets. Clift, Grace & Weber (1978) also give a review on this subject.

Considering higher-Reynolds-number flow, Hamielec & Johnson (1962) and later Hamielec, Storey & Whitehead (1963) used a Galerkin treatment to obtain polynomial solutions for ratios of inside to outside viscosity from 0 to 10^5 , and the effects of interior Reynolds numbers were not mentioned. Later, Nakano & Tien (1963) used a Galerkin treatment for a solution of similar flow conditions, adding to the work of Hamielec *et al.* an additional parameter of the inside Reynolds number. None of the above Galerkin methods were in good agreement with the Hadamard–Rybczynski solution at low-Reynolds-number flow because the trial functions do not contain the necessary term. Later, Abdel-Alim & Hamielec (1975) developed a solution for the drag of a fluid sphere, without regarding the interior Reynolds number. This solution was not in agreement with Hadamard (1911) and Rybczynski's (1911) creeping-flow solution. That was probably because the free-stream condition was not set far enough numerically from the droplet surface. The solution, however, was in agreement with their own experimentally determined drag coefficients with a density ratio of near unity for large Reynolds numbers. Rivkind, Ryskin & Fishbein (1976) have used ordinary finite-difference methods to solve for a limited number of viscosity ratios with exterior Reynolds numbers ranging from 0.5 to 200. They concluded that the drag coefficient for a fluid sphere could be approximated by

$$C_D = \frac{\Phi_\mu C_{D\infty} + C_{D0}}{\Phi_\mu + 1},$$

where Φ_μ is the ratio of the inside to outside viscosities, $C_{D\infty}$ is the drag coefficient of a solid sphere ($\Phi_\mu \rightarrow \infty$), and C_{D0} is the drag coefficient of a gas bubble in liquid ($\Phi_\mu \rightarrow 0$). They also concluded that, for exterior Reynolds numbers ranging between 5 and 100, the interior Reynolds number has an insignificant effect on the drag coefficient. Rivkind & Ryskin (1976) published another paper of a similar account. The calculated drag coefficients of the later publication appear to approach asymptotically the predicted creeping-flow solution.

In the published literature on the motion of a fluid sphere as reviewed above, mainly extreme cases like flow over a solid sphere ($\Phi_\mu = \mu_1/\mu_0 \rightarrow \infty$) and flow over a gas bubble ($\Phi_\mu \rightarrow 0$) have been investigated, whereas, for low- but finite-Reynolds-number flow, little work has been done. This paper is intended to help fill this gap for the low-Reynolds-number flow by analysing the effects of viscosity and density ratios in the fluid flow.

2. Basic Assumptions

(a) The droplet remains spherical (Rivkin *et al.* (1976) cite experimental evidence that droplets stay reasonably spherical if the Weber number is below 0.1).

(b) Both fluids are Newtonian and mutually immiscible, and there is no chemical reaction.

(c) The system involves only purified fluids (there are no surface-active materials).

(d) There is no interfacial mass transfer (the radial velocity is zero at the interface).

(e) Fluid properties are constant and the flow is steady.

3. Theoretical formulation

A fluid sphere of density ρ_1 , viscosity μ_1 is moving steadily in another fluid of density ρ_0 , viscosity μ_0 , and the internal motion is fully developed. The schematic representation of the physical model and coordinate system is shown in figure 1. The equation of continuity is satisfied by introducing the dimensionless stream function $\psi(\xi, \theta)$ defined by the following equations:

$$u_1 = \frac{1}{r^2 \sin \theta} \frac{\partial \psi_1}{\partial \theta}, \quad v_1 = \frac{-1}{r \sin \theta} \frac{\partial \psi_1}{\partial r} \quad (\text{interior}), \quad 0 \leq r \leq a; \quad (1a)$$

$$u_0 = \frac{e^{-2\xi}}{\sin \theta} \frac{\partial \psi_0}{\partial \theta}, \quad v_0 = \frac{-e^{-2\xi}}{\sin \theta} \frac{\partial \psi_0}{\partial \xi} \quad (\text{exterior}), \quad a < r; \quad (1b)$$

with

$$\xi = \ln r;$$

where the velocities are non-dimensionalized by the free-stream velocity U_∞ , ψ by $U_\infty a^2$, and r by the radius a . The other variable to be used is the dimensionless vorticity $\omega(r, \theta)$ defined by the equation

$$\omega_1 = \frac{\partial v_1}{\partial r} + \frac{v_1}{r} - \frac{1}{r} \frac{\partial u_1}{\partial \theta} \quad (\text{interior}), \quad 0 \leq r \leq 1, \quad (2)$$

$$\omega_0 e^\xi = \frac{\partial v_0}{\partial \xi} + v_0 - \frac{\partial u_0}{\partial \theta} \quad (\text{exterior}), \quad 1 < r.$$

The equations of motion satisfied by ψ_1 and ω_1 are then:

$$E^2 \psi_1 = -r (\sin \theta) \omega_1; \quad (3a)$$

$$\left[\frac{\partial \psi_1}{\partial r} \frac{\partial}{\partial \theta} \left(\frac{\omega_1}{r \sin \theta} \right) - \frac{\partial \psi_1}{\partial \theta} \frac{\partial}{\partial r} \left(\frac{\omega_1}{r \sin \theta} \right) \right] = \frac{2}{Re_1} \frac{1}{\sin \theta} E^2 (-r \omega_1 \sin \theta); \quad (3b)$$

where

$$E^2 = \frac{\partial^2}{\partial r^2} + \frac{\sin \theta}{r^2} \frac{\partial}{\partial \theta} \left(\frac{1}{\sin \theta} \frac{\partial}{\partial \theta} \right), \quad Re_1 = \frac{U_\infty \rho_1 2a}{\mu_1}.$$

The exterior equations of motion are given as:

$$\frac{\partial^2 \psi_0}{\partial \xi^2} - \frac{\partial \psi_0}{\partial \xi} + \sin \theta \frac{\partial}{\partial \theta} \left(\frac{1}{\sin \theta} \frac{\partial \psi_0}{\partial \theta} \right) = -\sin \theta e^{3\xi} \omega_0; \quad (4a)$$

$$u_0 \frac{\partial \omega_0}{\partial \xi} + v_0 \frac{\partial \omega_0}{\partial \theta} - u_0 \omega_0 - v_0 \omega_0 \cot \theta = \frac{2}{Re_0} e^{-\xi} \left(\frac{\partial^2 \omega_0}{\partial \xi^2} + \frac{\partial \omega_0}{\partial \xi} + \cot \theta \frac{\partial \omega_0}{\partial \theta} + \frac{\partial^2 \omega_0}{\partial \theta^2} - \frac{\omega_0}{\sin^2 \theta} \right); \quad (4b)$$

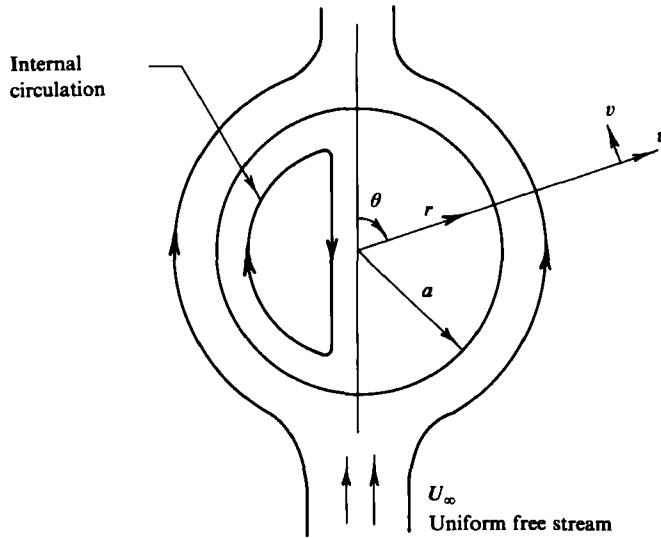


FIGURE 1. Schematic and coordinate system.

with
$$Re_o = Re_i \frac{\rho_o \mu_i}{\rho_i \mu_o}.$$

The boundary conditions to be satisfied are:

(I) At the interface $r = 1$,

$$v_i = v_o, \quad \text{continuity of tangential velocity,} \quad (5a)$$

$$u_i = u_o = 0, \quad \text{no mass transfer at the interface} \quad (5b)$$

(where the subscripts *i* and *o* denote the inside and outside parameters, respectively);

$$\mu_i(\omega_i - 2v_i) = \mu_o(\omega_o - 2v_o), \quad \text{equal shear stress,} \quad (6)$$

$$\psi_i(1) = \psi_o(0), \quad (7)$$

$$= 0.$$

(II) At the free stream $r \rightarrow \infty$,

$$\psi_o \rightarrow \frac{1}{2} e^{2\xi} \sin^2 \theta \quad \text{as } \xi \rightarrow \infty, \quad (8a)$$

$$\omega_o \rightarrow 0 \quad \text{as } \xi \rightarrow \infty, \quad (8b)$$

(III) At the sphere centre $r \rightarrow 0$,

$$\psi_i \rightarrow 0 \quad \text{as } r \rightarrow 0, \quad (9a)$$

$$\omega_i \rightarrow 0 \quad \text{as } r \rightarrow 0. \quad (9b)$$

4. Solution procedure

A very attractive numerical method due to Van Dyke (1965), which was developed for spherical geometry and low and moderate Reynolds numbers, has been shown to be effective from the point of both computer economy and calculation accuracy in the area of fluid motion and heat transfer around a solid sphere. This semi-analytical numerical procedure of series-truncation, spectral type of method, has been success-

fully used by Underwood (1969), Dennis & Walker (1971) and Dennis, Walker & Hudson (1973). They applied it to flows over cylinders and spheres and also for heat transfer to a sphere. This method is superior to the fully finite-difference schemes in that, at small and moderate Reynolds numbers, we not only solve very few terms, but we also deal with a set of ordinary differential equations instead of partial differential equations.

We first define the four dependent variables in terms of an unknown function of r , and Legendre or associated Legendre functions:

$$\psi_1 = \sum_{n=1}^{\infty} F_n(r) \int_z^1 P_n(t) dt; \quad \psi_0 = e^{\frac{1}{2}\xi} \sum_{n=1}^{\infty} f_n(\xi) \int_z^1 P_n(t) dt; \quad (10a, b)$$

$$\omega_1 = \sum_{n=1}^{\infty} G_n(r) P_n^1(z); \quad \omega_0 = \sum_{n=1}^{\infty} g_n(\xi) P_n^1(z); \quad (11a, b)$$

where $P_n(z)$ and $P_n^1(z)$ are the Legendre and first associated Legendre functions of order n , and $z = \cos \theta$. We have now defined the four variables in terms of a series of functions of radius (g_n, G_n, f_n, F_n) and of angle ($P_n(z), P_n^1(z)$). We now use the orthogonality of Legendre and associated Legendre functions to convert the partial differential equations (3 and 4) into ordinary differential equations of a series form. We note that

$$\int_z^1 P_n(t) dt = \frac{\sin \theta}{n(n+1)} P_n^1(z).$$

Substituting this into (10a, b), we obtain

$$\psi_1 = \sum_{n=1}^{\infty} F_n(r) \frac{\sin \theta}{n(n+1)} P_n^1(z); \quad \psi_0 = e^{\frac{1}{2}\xi} \sum_{n=1}^{\infty} f_n(\xi) \frac{\sin \theta}{n(n+1)} P_n^1(z). \quad (12a, b)$$

Substituting (12) into (1), we obtain:

$$u_1 = \sum_{n=1}^{\infty} \frac{F_n(r)}{r^2} P_n(z); \quad u_0 = e^{-\frac{3}{2}\xi} \sum_{n=1}^{\infty} f_n(\xi) P_n(z). \quad (13a, b)$$

$$v_1 = \sum_{n=1}^{\infty} -\frac{F'_n(r)}{r} \frac{1}{n(n+1)} P_n^1(z); \quad (14a)$$

$$v_0 = -e^{-\frac{3}{2}\xi} \sum_{n=1}^{\infty} \left(f'_n(\xi) + \frac{f_n(\xi)}{2} \right) \frac{1}{n(n+1)} P_n^1(z). \quad (14b)$$

Substituting these into (3a) and (4b) using the orthogonality of the Legendre functions gives

$$F_n'' - \frac{n(n+1)}{r^2} F_n = -rn(n+1) G_n; \quad f_n'' - (n + \frac{1}{2})^2 f_n = -e^{\frac{1}{2}\xi} n(n+1) g_n. \quad (15a, b)$$

Boundary conditions (5)–(9) become:

$$F'_n(1) = f'_n(0); \quad (16)$$

$$F_n(1) = f_n(0) = 0; \quad (17)$$

$$\Phi_\mu \left(G_n(1) + \frac{2F'_n(1)}{n(n+1)} \right) = \left(g_n(0) + \frac{2f'_n(0)}{n(n+1)} \right); \quad (18)$$

$$F_n(r) \rightarrow 0 \quad \text{as } r \rightarrow 0; \quad (19)$$

$$G_n(r) \rightarrow 0 \quad \text{as } r \rightarrow 0. \quad (20)$$

The boundary conditions at the outer edge of the external flow ($\xi \rightarrow \infty$) are given as follows:

$$f_n(\xi) \rightarrow e^{i\xi} \delta_{n1} \quad \text{as } \xi \rightarrow \infty, \tag{21}$$

where δ_{n1} is the Kronecker delta.

$$g_n(\xi) \rightarrow 0 \quad \text{as } \xi \rightarrow \infty. \tag{22}$$

Substituting in the appropriate series into (3b) and (4b) yields:

$$\begin{aligned} & \sum_{n=1}^{\infty} [r^2 G_n'' + 2rG_n' - n(n+1)G_n] P_n^1 \\ &= \frac{1}{2} Re_1 \left[\sum_{n=1}^{\infty} \sum_{i=1}^{\infty} \left(\frac{F_n P_n}{r} (rG_i' - G_i) P_i^1 + \frac{F_n' P_n^1}{n(n+1)} G_i P_i^2 \right) \right]. \end{aligned} \tag{23a}$$

$$\begin{aligned} & \sum_{n=1}^{\infty} [g_n'' + g_n' - n(n+1)g_n] P_n^1 \\ &= \frac{1}{2} Re_0 e^{-i\xi} \left[\sum_{n=1}^{\infty} \sum_{i=1}^{\infty} \left(f_n P_n (g_i' - g_i) P_i^1 + \frac{f_n' + f_n/2}{n(n+1)} P_n^1 g_i P_i^2 \right) \right]. \end{aligned} \tag{23b}$$

Talman (1968) gives a method of transforming a product of Legendre functions into a series of a single Legendre or Associated Legendre functions, using the Wigner ‘3-*J*’ coefficients. Rottenberg *et al.* (1959) present an overview of the theory of ‘3-*J*’ coefficients as they relate to spherical harmonics.

Combining all products of Legendre and Associated Legendre functions (after Talman 1968), then using the orthogonality of these functions, we rid (23a, b) of all Legendre functions. Hence we are left with ordinary differential equations:

$$r^2 G_n'' + 2rG_n' - n(n+1)G_n = S_{n1}, \quad g_n'' + g_n' - n(n+1)g_n = S_{n0}, \tag{24a, b}$$

where

$$\left. \begin{aligned} S_{n1} &= \frac{1}{2} \frac{Re_1}{r} \left[\sum_{i=1}^{\infty} \sum_{j=1}^{\infty} (\alpha_{i,j}^n F_i(G_j' r - G_j) + \beta_{i,j}^n r F_i' G_j) \right], \\ S_{n0} &= \frac{1}{2} Re_0 e^{-i\xi} \left[\sum_{i=1}^{\infty} \sum_{j=1}^{\infty} (\alpha_{i,j}^n f_i(g_j' - g_j) + \beta_{i,j}^n (f_i' + \frac{1}{2} f_i) g_j) \right], \end{aligned} \right\} \tag{25a}$$

$$\left. \begin{aligned} \alpha_{i,j}^n &= -(2n+1) \left[\frac{j(j+1)}{n(n+1)} \right]^{\frac{1}{2}} \begin{pmatrix} n & i & j \\ -1 & 0 & 1 \end{pmatrix} \begin{pmatrix} n & i & j \\ 0 & 0 & 0 \end{pmatrix}, \\ \beta_{i,j}^n &= (2n+1) \left[\frac{j(j^2-1)(j+2)}{n(n+1)i(i+1)} \right]^{\frac{1}{2}} \begin{pmatrix} n & i & j \\ -1 & -1 & 2 \end{pmatrix} \begin{pmatrix} n & i & j \\ 0 & 0 & 0 \end{pmatrix}, \end{aligned} \right\} \tag{25b}$$

with

$$\begin{pmatrix} j_1 & j_2 & j_3 \\ m_1 & m_2 & m_3 \end{pmatrix}$$

being the Weigner ‘3-*J*’ symbol.

Equations (24a) and (24b) are now truncated by setting $F_n = G_n = f_n = g_n = 0$ for all $n > n_0$. Where n_0 is dependent upon the Reynolds number, as Re_0 becomes larger n_0 does also. This is the main limiting factor for the upper bound of Reynolds numbers as Brabston & Keller (1975) state that the computation time for their scheme was proportional to n_0^3 . The actual value of n_0 must be found through trial and error by increasing n_0 for each Reynolds number until convergence is assumed. As an example, Dennis & Walker (1971) used $n_0 = 6$ for $Re_0 \leq 1$ but $n_0 = 20$ for $Re_0 = 40$.

We have set $n_0 = 4$, for $Re_0 \leq 1.0$. The choice of $n_0 = 4$ for this analysis is further discussed in §5.

The main advantage of the series truncation method arises from the fact that the problem is reduced to the solution of ordinary differential equations. First, the necessity of approximating derivatives in the direction by finite differences is avoided. This is known to present difficulties in the far-wake region behind the sphere, and it may cause computation instability inside the fluid sphere. According to Dennis & Walker (1971), this method uses less computer core storage compared to fully finite-difference methods. Therefore, the series, truncation method is best suited for the flows in the low- and moderate-Reynolds-number range where only a few terms are required for good accuracy.

Equations (24*a*) and (24*b*) in their truncated form and the associated boundary conditions (18), (20) and (22) present a set of boundary-value problem equations. We define (24*a*) and (24*b*) as the vorticity equations and (15*a*) and (15*b*) as the stream-function equations. The particular equation for a given value of n is called the n th mode.

These equations were solved iteratively from $n = 1$ to $n = n_0$, one mode at a time, holding the values of all parameters in other modes constant until all boundary conditions were satisfied for this given mode. We then relaxed the parameters of this mode and performed the same operation on the next mode. During the above primary iteration the nonlinear terms (the ' S_n ' terms) were held constant. At the end of each primary-iteration cycle the nonlinear terms were relaxed and the primary-iteration cycle was then repeated until convergence requirement was satisfied.

Finite-difference methods were used to calculate all derivatives with a tridiagonal matrix algorithm used to solve both the vorticity and the stream-function equations. Use of these methods presented instability problems as the Reynolds number was increased. This was remedied by setting all nonlinear terms equal to zero for all $\xi \geq 3.96$ and setting $\xi_\infty = 5.5$, at which the free-stream conditions were assumed. The justification for this is based on an analysis that the error due to the neglect of the nonlinear terms is of the order ($Re_0/\exp(\xi)$) which is acceptable in this study.

For most of the computations, the interior nonlinear terms were neglected, i.e. $Re_i = 0$. Computations were also performed including the interior nonlinear terms to investigate the effects of non-zero Re_i . We varied the interior Reynolds number from near zero to two orders of magnitude greater than that of the exterior Reynolds number. This variation of Re_i was performed from $Re_0 = 0.1$ to $Re_0 = 1.0$ and it had a negligible effect on the drag coefficient.

These calculations were performed on a Prime 400 computer. We used 40 interior and 196 exterior node points in performing the computations, with the exception of the solid-sphere calculation where 147 exterior nodal points were used. Also, when plotting the parameters, more interior nodes were used to obtain better resolution near the centre.

5. Results and comparisons

We will use primarily the drag coefficient as a means of reporting and comparing our results. Results obtained are compared with analytical creeping-flow solutions, those of Dennis & Walker (1971) for solid spheres, and those of Brabston (1974) for gas bubbles. The drag coefficient C_D is defined as

$$C_D = \frac{F}{\pi \rho_0 U_\infty^2 a^2}, \quad (26)$$

where F is the drag force and ρ_0 is the exterior density. Brabston (1974) gives the following as the drag coefficient for a fluid sphere without any interfacial mass transfer:

$$C_D = -e^{2\xi} \left[\int_0^\pi P(\xi, \theta) \sin 2\theta \, d\theta + \frac{4}{Re_0} \int_0^\pi \omega(\xi, \theta) \sin^2 \theta \, d\theta - 2 \int_0^\pi uv \sin^2 \theta \, d\theta + \int_0^\pi u^2 \sin 2\theta \, d\theta \right], \quad (27)$$

where $P(\xi, \theta)$ is pressure.

We evaluate this coefficient only at the interface, hence the u terms are zero for the current case of no interfacial mass transfer, leaving, after much manipulation,

$$C_D(f) = -\frac{16}{3Re_0} g_1(0),$$

$$C_D(p) = \frac{8}{3Re_0} [g'_1(0) + g(0)]$$

$$-4 \sum_{i=1}^{\infty} f'_i(0) f'_{i+1}(0) \left[\frac{1}{i(i+1)^2(i+2)} \right]^{\frac{1}{2}} \begin{pmatrix} 1 & i & i+1 \\ 0 & 1 & -1 \end{pmatrix} \begin{pmatrix} 1 & i & i+1 \\ 0 & 0 & 0 \end{pmatrix}, \quad (28)$$

where

$$C_D = C_D(f) + C_D(p),$$

with $C_D(f)$ and $C_D(p)$ being the drag coefficients due to friction and pressure, respectively. This derivation is obtained by integrating the pressure (as given in the Navier–Stokes equation) and the vorticity around the surface of the droplet. The drag on the fluid sphere can be calculated from a knowledge of $g_n(0)$, $g'_n(0)$, $f_n(0)$ and $f'_n(0)$. These coefficients are given in tables 1 and 2 for some typical cases.

As seen from tables 1 and 2, the absolute values of g_n , g'_n , and f'_n drop dramatically as n increases. This is the chief reason that $n_0 = 4$ is adopted in this study. $n_0 = 6$ has been applied to some cases, but the improvement did not show up in the results because the improvement is of the order of the convergence criterion.

For comparison with the analytical creeping-flow solution, the value of C_D for $Re_0 \rightarrow 0$ is given as

$$C_{D0} = \frac{8}{Re_0} \left[\frac{1 + 1.5\Phi_\mu}{1 + \Phi_\mu} \right]. \quad (29)$$

For example, with a solid sphere, $\Phi_\mu \rightarrow \infty$, C_D is equal to $12/Re_0$. Both Brabston (1974) and Dennis & Walker (1971) have calculated the drag coefficients for the special case of a solid sphere. The comparison is shown in table 3, with much of the variation due to the use of different ξ_∞ values, where the free-stream condition is set. Other factors such as step size, convergence criterion, and type of computer would also contribute to the slight differences.

We will examine next the effect of density ratios, $\Phi_\mu = \rho_1/\rho_0$, on the drag coefficient. The results obtained are for the case of $\Phi_\rho/\Phi_\mu = 100$, i.e. $Re_1 = 100Re_0$, which covers the range of the most practical applications because Φ_μ and Φ_ρ cannot be varied arbitrarily for realistic material. In table 4, Φ_μ varying from 0.1 to 10 corresponds to Φ_ρ going from 10 to 10^3 . The drag coefficient for the pseudo-physical case of the same Re_0 and Φ_μ but zero Φ_ρ is also shown in the parenthesis for the purpose of comparison. It is apparent that the variation of the density ratios has almost no effect on the drag coefficient. Due to the insensitivity of C_D with Φ_ρ , most of the sample calculations presented here were done under the condition of $Re_1 = 0$.

Re_o	Φ_μ	g_1	g_2	g_3	g_4
0.1	0.333	-1.1376	0.0059	0.9008×10^{-6}	0.6772×10^{-8}
	1.00	-1.2656	0.0079	0.9747×10^{-6}	0.9403×10^{-8}
	3.0	-1.3935	0.0099	0.9501×10^{-6}	0.1424×10^{-7}
	∞	-1.5214	0.0120	0.8908×10^{-6}	0.2108×10^{-7}
0.5	0.333	-1.1910	0.0280	0.1984×10^{-3}	0.1179×10^{-5}
	1.0	-1.3309	0.0376	0.2077×10^{-3}	0.1650×10^{-5}
	3.0	-1.4718	0.0475	0.1920×10^{-3}	0.2397×10^{-5}
	∞	-1.6136	0.0574	0.1671×10^{-3}	0.3367×10^{-5}
1.0	0.333	-1.2521	0.0528	0.6541×10^{-3}	0.9451×10^{-5}
	1.0	-1.4048	0.0715	0.6426×10^{-3}	0.1305×10^{-4}
	3.0	-1.5622	0.0907	0.5269×10^{-3}	0.1865×10^{-4}
	∞	-1.7176	0.1098	0.3730×10^{-3}	0.2597×10^{-4}
Re_o	Φ_μ	g'_1	g'_2	g'_3	g'_4
0.1	0.333	2.2734	-0.0218	0.7333×10^{-6}	-0.7859×10^{-7}
	1.0	2.5293	-0.0276	0.1130×10^{-5}	-0.1224×10^{-6}
	3.0	2.7849	-0.0334	0.1776×10^{-5}	-0.1713×10^{-6}
	∞	3.0404	-0.0390	0.2395×10^{-5}	-0.2163×10^{-6}
0.5	0.333	2.3823	-0.1067	0.7792×10^{-4}	-0.4910×10^{-5}
	1.0	2.6616	-0.1347	0.1349×10^{-3}	-0.1078×10^{-4}
	3.0	2.9429	-0.1627	0.2009×10^{-3}	-0.1742×10^{-4}
	∞	3.2263	-0.1898	0.2029×10^{-3}	-0.2356×10^{-4}
1.0	0.333	2.5112	-0.2080	0.6737×10^{-3}	-0.3904×10^{-4}
	1.0	2.8160	-0.2629	0.1157×10^{-2}	-0.8362×10^{-4}
	3.0	3.1278	-0.3165	0.1610×10^{-2}	-0.1340×10^{-3}
	∞	3.4418	-0.3694	0.1915×10^{-2}	-0.1793×10^{-3}

TABLE 1. Values of $g_n(0)$ and $g'_n(0)$ for $Re_1 = 0$

Re_o	Φ_μ	f'_1	f'_2	f'_3	f'_4
0.1	0.333	0.7575	-0.0096	-0.2477×10^{-4}	-0.2677×10^{-7}
	1.0	0.5048	-0.0067	-0.1285×10^{-4}	-0.1681×10^{-7}
	3.0	0.2524	-0.0035	-0.4893×10^{-5}	-0.9699×10^{-8}
	∞	0.0000	0.0000	0.0000	0.0000
0.5	0.333	0.7916	-0.0456	-0.5455×10^{-3}	-0.4664×10^{-5}
	1.0	0.5309	-0.0320	-0.2739×10^{-3}	-0.2949×10^{-5}
	3.0	0.2671	-0.0166	-0.9886×10^{-4}	-0.1620×10^{-5}
	∞	0.0000	0.0000	0.0000	0.0000
1.0	0.333	0.8333	-0.0860	-0.1805×10^{-2}	-0.3739×10^{-4}
	1.0	0.5603	-0.0609	-0.8473×10^{-3}	-0.2332×10^{-4}
	3.0	0.2820	-0.0319	-0.2670×10^{-3}	-0.1267×10^{-4}
	∞	0.0000	0.0000	0.0000	0.0000

TABLE 2. Values of $f'_n(0)$ for $Re_1 = 0$

Moreover, table 4 also demonstrates the variation of viscosity ratios on the drag coefficients for low-Reynolds-number flows. The drag coefficients decrease with increasing Re_o but increase with increasing Φ_μ .

Table 5 again shows the effects of viscosity ratio with a complete spectrum of Φ_μ . These results are also plotted in figure 2 with drag coefficient normalized by

Re_0	Present results		Brabston (1974)	Dennis & Walker (1971)
	$\xi_\infty = 4.9$	$\xi_\infty = 5.5$	$\xi_\infty = 4.9$	$\xi_\infty = 4.9$
0.1	122.31	121.65	122.10	122.10
0.2	61.97	61.71	—	62.02
0.5	25.87	25.82	25.74	25.85
0.8	16.82	16.79	—	16.76
1.0	13.78	13.76	13.72	13.72

TABLE 3. Drag coefficient for $\Phi_\mu = \infty$ (solid sphere)

Re_0	$\Phi_\mu = 0.1, \Phi_\rho = 10$	$\Phi_\mu = 1.0, \Phi_\rho = 100$	$\Phi_\mu = 10.0, \Phi_\rho = 10^3$
0.1	84.46 (84.46)	101.20 (102.20)	117.93 (117.93)
0.5	17.64 (17.63)	21.30 (21.30)	24.99 (24.99)
0.7	12.85 (12.84)	15.57 (15.57)	18.32 (18.30)
0.9	— —	12.38 (12.38)	— —

TABLE 4. Comparison of drag coefficients for $Re_1 = 0$ with those for $Re_1 = 100Re_0$ (the latter being in parentheses)

Re_0	$\Phi_\mu = 0.0\dagger$	$\Phi_\mu = 0.10$	$\Phi_\mu = 0.333$	$\Phi_\mu = 1.00$	$\Phi_\mu = 3.0$	$\Phi_\mu = 10.0$	$\Phi_\mu = \infty\dagger$
0.1	80.83	84.46	90.97	101.20	111.43	117.93	121.65
0.2	—	—	45.99	51.23	56.46	—	61.71
0.3	—	28.78	31.04	34.61	38.20	40.48	41.80
0.4	—	—	23.55	26.29	29.04	—	31.81
0.5	16.85	17.64	19.06	21.30	23.55	24.99	25.82
0.6	—	—	16.06	17.96	19.87	—	21.82
0.7	—	12.85	13.90	15.57	17.24	18.32	18.94
0.8	—	—	12.29	13.77	15.28	—	16.79
0.9	—	10.20	11.03	12.38	13.74	14.60	15.11
1.0	8.795	—	10.03	11.25	12.51	—	13.76

† Gas bubble, Brabston (1974).

‡ Solid sphere, present solution.

TABLE 5. Drag coefficients for various Φ_μ with $Re_1 = 0$

creeping-flow drag, i.e. (29). The curves in figure 2 have been best-fitted with the following equation:

$$C_D = C_{D0} + 0.0126(C_{D0} Re_0)^2. \tag{30}$$

The trends that C_D is almost independent of Φ_ρ but is strongly dependent on Φ_μ and Re_0 may be explained from the continuity of shear stress at the interface which induces the motion inside the fluid sphere. The higher the Φ_μ , the larger the internal resistance to motion and, therefore, the larger the C_D values. Inside the droplet, the magnitude of the velocities is always significantly lower than that of the free-stream velocities as seen in figure 4 and Φ_ρ is only involved through (25a), the nonlinear momentum flux term, which is at least one order of magnitude smaller than the viscous term at low Reynolds number. Therefore, one would expect Φ_ρ to have a lesser effect on the drag coefficient. We can also predict from these two equations that C_D

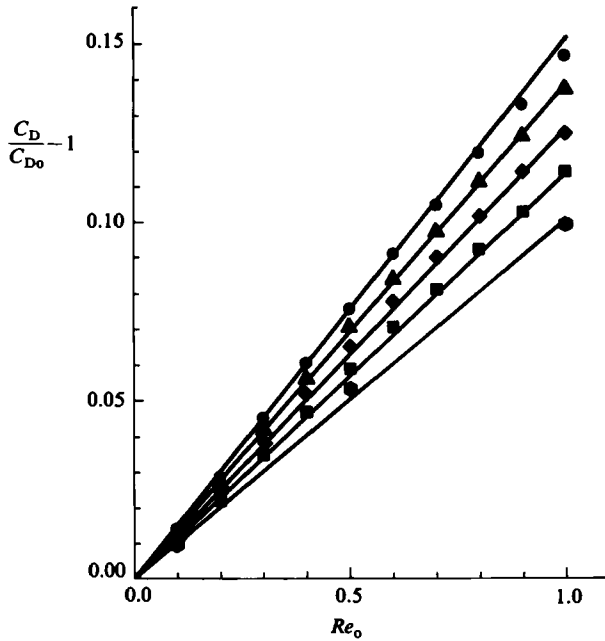


FIGURE 2. Ratio of drag coefficient to that of creeping flow as a function of Re_0 and Φ_μ . Calculated values: \bullet , $\Phi_\mu = \infty$; \blacktriangle , $\Phi_\mu = 3$; \blacklozenge , $\Phi_\mu = 1$; \blacksquare , $\Phi_\mu = 0.333$; \bullet , $\Phi_\mu = 0$. Data lines $C_D = C_{D0} + 0.0126(C_{D0} Re_0)^2$.

Re_0	$\Phi_\mu = 0.1$	$\Phi_\mu = 1.0$	$\Phi_\mu = 10.0$
0.1	0.6670	0.6670	0.6670
0.3	0.6669	0.6669	0.6669
0.5	0.6667	0.6667	0.6667
0.7	0.6665	0.6665	0.6665
0.9	0.6662	0.6662	0.6662

TABLE 6. Ratio of friction drag to total drag

Φ_μ	Present results	Abdel-Alim & Hamielec (1975)
0.0995	9.24	8.75
0.3010	9.93	9.60
0.5540	10.55	10.01

TABLE 7. Comparison of drag coefficient for $Re_0 = 1$

does not depend on Φ_ρ . The ratio of friction drag to total drag varies only slightly with Re_0 as shown in table 6. Friction drag is about twice as large as the pressure drag. Comparisons were also made in table 7 between the current results and those of Abdel-Alim & Hamielec (1975) at $Re_0 = 1$ for various Φ_μ . Abdel-Alim and Hamielec (1975) predict drag consistently lower by 5%. The differences are thought probably to be due to their not posting the free-stream condition far enough from the interface

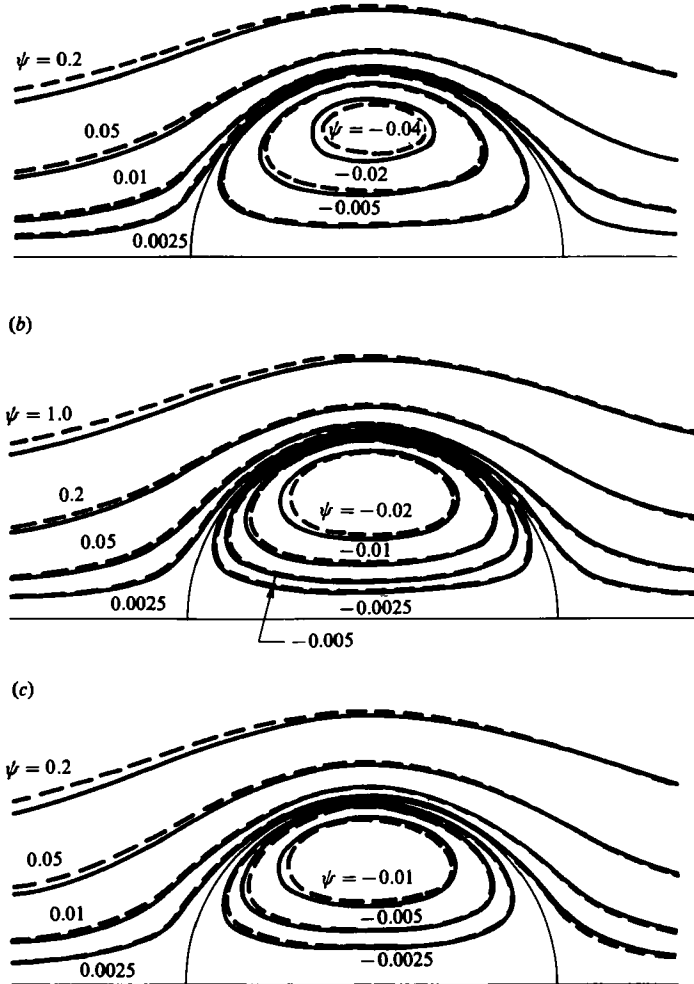


FIGURE 3. Stream-function contours for $Re_0 = 0.7$ and (a) $\Phi_\mu = 0.333$, (b) $\Phi_\mu = 1.0$, and (c) $\Phi_\mu = 3.0$: —, current calculations; ···, H-R solutions.

in their finite-difference numerical procedure. They set the free-stream condition at a distance of 28.5 radii from the interface, while ours is at 245 radii.

Figure 3 plots the stream-function contours for $Re_0 = 0.7$ and different viscosity ratios. The dotted lines represent the creeping-flow solutions. The inertia effect on the streamlines is significant only in the upstream of the fluid sphere for the external flows and two streamlines almost coincide with each other after the equator. This is thought to be related to the fact that the vorticity and the pressure gradient are higher in magnitude in the upstream ($90^\circ < \theta < 180^\circ$) than those in the downstream. The variations of the tangential velocity and the pressure coefficient, $K(\theta)$, over the surface of the sphere are shown in figures 4 and 5.

The pressure coefficient is defined as:

$$\begin{aligned}
 K(\theta) &= \frac{p(\theta) - P_\infty}{\frac{1}{2}\rho_0 U_\infty^2} \\
 &= K(\pi) - v_\theta^2 + \frac{4}{Re_0} \sum_{n=1}^{\infty} [g_n(0) + g'_n(0)] [P_n(\cos \theta) - (-1)^n],
 \end{aligned}$$

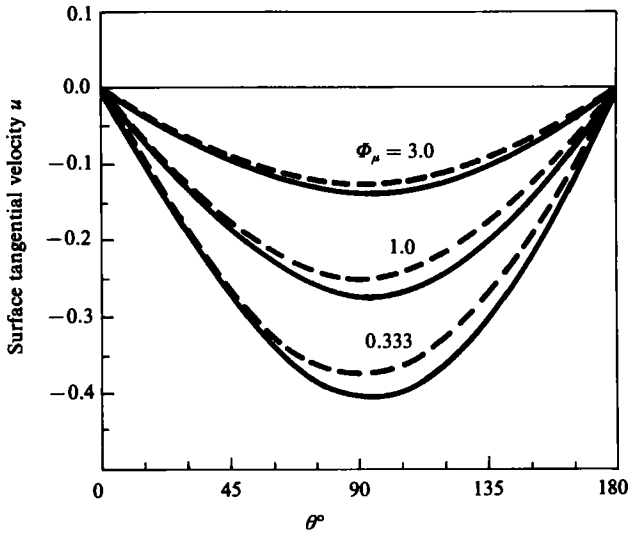


FIGURE 4. Tangential velocity at the interface for $Re_o = 0.7$ and $\Phi_\mu = 0.333, 1.0,$ and 3.0 ; —, current calculations; ---, H-R solutions.

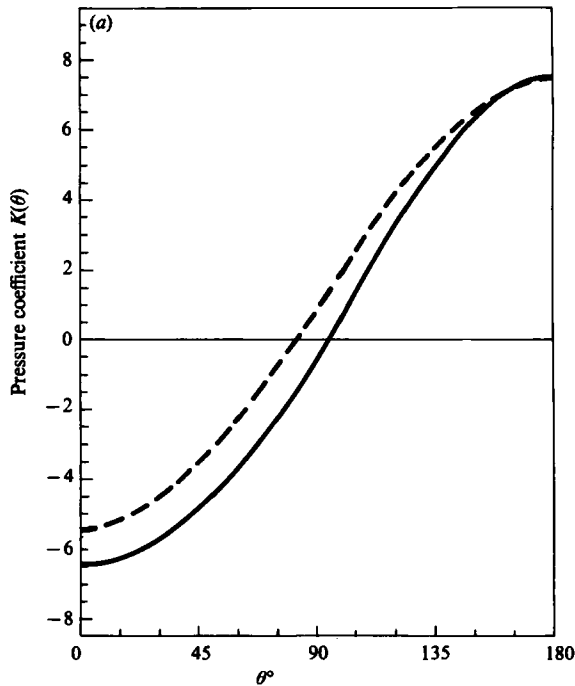


FIGURE 5(a). For caption see p. 228.

where

$$K(\pi) = 1 + \frac{4}{Re_o} \sum_{n=1}^{\infty} (-1)^n n(n+1) \int_0^{\infty} g_n(\xi) d\xi.$$

$P(\theta)$ and P_∞ are pressures on the surface of the sphere and far away from the sphere, respectively. Therefore, the inclusion of the inertia term may more sensitively contribute to the force balance in the upstream part of the fluid sphere.

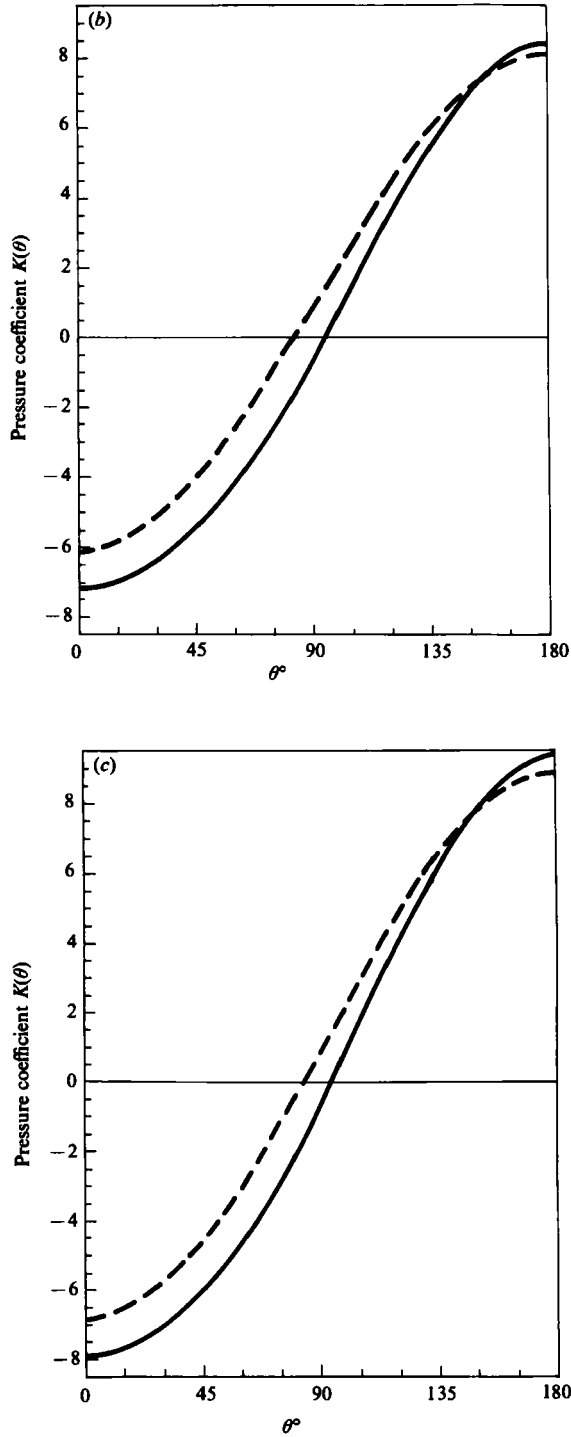


FIGURE 5. Pressure coefficient over the surface of the fluid sphere for $Re_o = 0.7$ and (a) $\Phi_\mu = 0.333$, (b) $\Phi_\mu = 1.0$, and (c) $\Phi_\mu = 3.0$: —, current calculations; ----, H-R solutions.

After examining the pressure distributions in figures 5(a-c), it is plausible to note that the pressure is very insensitive to the variation of Φ_μ . The deformation tendency is small because the pressure hardly deviates from that of Hadamard-Rybczynski. Based on the pressure changes along the interface, the droplet will tend to deform into an oblate spheroid or a spherical cap. The above observations are consistent with the results of Taylor & Acrivos (1964), who found, by singular perturbation technique, that the deformation is of the order of Re_0^2 and is insensitive to Φ_μ at low Reynolds number.

6. Conclusion

It may be concluded that, for the ratios studied, the observations of Nakano & Tien (1963) that the density ratio has little effect on the drag coefficient are valid. Also, the ratio of pressure-induced drag to that induced by friction is nearly constant at 1:2.

In general, the ratio of the drag coefficient to the drag coefficient for the creeping-flow solution increases nearly linearly with the largest deviation for the solid sphere, and the smallest for a gas bubble. The drag coefficient may be well correlated by the equation

$$C_D = C_{D_0} + 0.0126(C_{D_0} Re_0)^2.$$

We wish to acknowledge the financial support received through the Washington State University Grant-in-Aid program.

REFERENCES

- ABDEL-ALIM, A. H. & HAMIELEC, A. E. 1975 *Ind. Engng Chem. Fund.* **14**, 308.
 BEARD, K. V. & PRUPPACHER, H. R. 1969 *J. Atmos. Sci.* **26**, 1066.
 BRABSTON, D. C. 1974 Numerical solution of steady viscous flow past spheres and gas bubbles. Ph.D. thesis, Calif. Inst. of Tech.
 BRABSTON, D. C. & KELLER, H. B. 1975 *J. Fluid Mech.* **69**, 179.
 CHAO, B. T. 1962 *Phys. Fluids* **5**, 69.
 CHESTER, W. & BREACH, D. K. 1969 *J. Fluid Mech.* **37**, 751.
 CLIFT, R., GRACE, J. R. & WEBER, M. E. 1978 *Bubbles, Drops and Particles*, Chap. 3 and 5. Academic.
 DENNIS, S. C. R. & WALKER, J. D. A. 1971 *J. Fluid Mech.* **48**, 771.
 DENNIS, S. C. R., WALKER, J. D. A. & HUDSON, J. D. 1973 *J. Fluid Mech.* **60**, 273.
 DENNIS, S. C. R. & WALKER, M. S. 1964 *Aero. Res. Council* no. **26**, 105.
 HADAMARD, J. 1911 *C.K. Acad. Sci.* **152**, 1735.
 HAMIELEC, A. E., HOFFMAN, T. Q. & ROSS, L. L. 1967 *AIChE J.* **12**, 212.
 HAMIELEC, A. E. & JOHNSON, A. I. 1962 *Can. J. Chem. Engng* **40**, 246.
 HAMIELEC, A. E., STOREY, A. E. & WHITEHEAD, J. M. 1963 *Can. J. Chem. Engng* **41**, 246.
 HARPER, J. F. 1972 *Adv. Appl. Mech.* **12**, 59.
 HARPER, J. F. & MOORE, D. W. 1968 *J. Fluid Mech.* **32**, 369.
 LECLAIR, B. P., HAMIELEC, A. E. & PRUPPACHER, H. R. 1970 *J. Atmos. Sci.* **27**, 308.
 McDONALD, J. E. 1954 *J. Met.* **11**, 478.
 MAXWORTHY, T. 1965 *J. Fluid Mech.* **23**, 369.
 MOORE, D. W. 1963 *J. Fluid Mech.* **16**, 161.
 NAKANO, Y. & TIEN, C. 1963 *Can. J. Chem. Engng* **41**, 135.
 PRAKASH, S. & SIRIGNANO, W. A. 1980 *Intl J. Heat Mass Transfer* **21**, 885.

- PROUDMAN, I. & PEARSON, J. R. A. 1957 *J. Fluid Mech.* **2**, 237.
- PRUPPACHER, H. R. & BEARD, K. V. 1970 *Q. J. R. Met. Soc.* **96**, 247.
- PRUPPACHER, H. R. & KLETT, J. D. 1978 *Microphysics of the Clouds and Circulation*. Reidel.
- PRUPPACHER, H. R., LECLAIR, B. P. & HAMIELEC, A. E. 1970 *J. Fluid Mech.* **44**, 781.
- PRUPPACHER, H. R. & STEINBERGER, E. H. 1968 *J. Appl. Phys.* **39**, 4129.
- RIVKIND, V. YA. & RYSKIN, G. M. 1976 *Fluid Dyn.* **11**, 5.
- RIVKIND, V. YA., RYSKIN, G. M. & FISHBEIN, G. A. 1976 *Appl. Math. Mech.* **40**, 687.
- ROTTENBERG, M., BIVINS, R., METROPOLIS, N. & WOOTEN, J. K. 1959 *The 3-J and 6-J Symbols*. MIT, Cambridge: The Technology Press.
- RYBCZNSKI, W. 1911 *Bull. Int. Acad. Pol. Sci. Lett. Cl. Sci. Math. Natur., Ser. A*, 40.
- TALMAN, J. D. 1968 *Special Functions*. Benjamin.
- TAYLOR, T. D. & ACRIVOS, A. 1964 *J. Fluid Mech.* **18**, 466.
- UNDERWOOD, R. L. 1969 *J. Fluid Mech.* **37**, 95.
- VAN DYKE, M. D. 1965 *Stanford University SUDAER* 247.
- WINNIKOW, S. & CHAO, B. T. 1965 *Phys. Fluids* **9**, 50.